A novel high-throughput framework to quantify spatio-temporal tumor clonal dynamics

Selami Baglamis[1,2,3,4], Joyaditya Saha[1,2,3,4], Maartje van der Heijden[1,2,3,4], Daniël M. Miedema[1,2,3,4], Démi van Gent[1,2,3,4], Przemek M. Krawczyk[2,5], Louis Vermeulen[1,2,3,4], and Vivek M Sheraton[1,2,3,4]

[1] Laboratory for Experimental Oncology and Radiobiology, Center for Experimental and Molecular Medicine, Amsterdam University Medical Centers (location AMC), Amsterdam, The Netherlands
[2] Cancer Center Amsterdam, Amsterdam, The Netherlands
[3] Oncode Institute, Amsterdam, The Netherlands
[4] Amsterdam Gastroenterology Endocrinology Metabolism, Amsterdam, The Netherlands
[5] Department of Medical Biology, Amsterdam University Medical Centers (location AMC), The Netherlands v.s.muniraj@amsterdamumc.nl

Abstract. Clonal proliferation dynamics within a tumor channels the course of tumor growth, drug response and activity. A high-throughput image screening technique is required to analyze and quantify the spatiotemporal variations in cell proliferation and influence of chemotherapy on clonal colonies. We present two protocols for generating spatial, Lentiviral Gene Ontology (LeGO) fluorescent tag based , mono- and co-culture systems with provisions for spatio-temporal tracking of clonal growth at the nucleus- and cytoplasm-level. The cultured cells are subjected to either drug treatment or co-cultured with fibroblasts and analyzed with a novel image processing framework. This framework enables alignment of cell positions based on motion capture techniques, tracking through time and investigation of drug actions or co-culturing on individual cell colonies. Finally, utilizing this framework, we develop agent-based models to simulate and predict the effects of the microenvironment and clonal density on cell proliferation. The model and experimental findings suggest growth stimulating effects of local clonal density irrespective of overall cell confluency.

Keywords: LeGO · cell tracking · diffusion dynamics · agent-based model

1 Introduction

Multicellular organisms exhibit complex biological phenomena. In order to delineate the biological processes associated with the observed phenomena, it is imperative to study them at the cellular level. In recent years, increasing emphasis is being placed on tracking specific populations of cells found to be enriched in a range of physiological and pathological conditions [4][12]. Temporal tracking of

ICCS Camera Ready Version 2023
To cite this paper please use the final published version:
DOI: 10.1007/978-3-031-36024-4_28

cells constituting different clones enables a greater understanding of associated clonal dynamics [15].

A range of factors influences clonal dynamics. The abundance of nutrients such as amino acids, nucleotides, lipids, and glucose influences the metabolic profiles of cells constituting clones which in turn influences their phenotype and dynamics [20]. While the role of nutrients on clonal dynamics has been studied extensively, in recent times, increasing attention is being directed to the role of cellular communication within and between clones. It is observed that cell-cell interactions often induce the activation of pathways favoring the establishment of unique cellular phenotypes that promote survival [10]. For instance, it is observed that cancer stem cells communicate with each other via Connexin46 (Cx46) gap junction proteins to synchronize biological processes such as cellular growth and proliferation. Disruption of the Cx46 gap protein specific cell-cell communication induces apoptosis in cancer stem cells [9].

In addition to cell-cell interactions taking place within the same population of cells, interactions can also occur between distinct populations of cells. Fibroblasts, in particular, are implicated to play a crucial role in the development of multiple pathologies such as cancer and rheumatoid arthritis (RA) [20][3][16]. The mechanisms via which fibroblasts promote the development and progression of tumors has been the focus of intense research and as such have been well documented. Fibroblast-cancer cell interactions are bi-directional [16]. Cancer-associated fibroblasts (CAFs), can either be tumor promoting or suppressive based on their interactions with cancer cells. In a recent study, it was observed that pancreatic cancer cells with a gain-of-function (GOF) mutant p53 interacted with CAFs in a paracrine manner via NF-κB signaling [16]. This paracrine interaction mediated by NF-κB signaling results in increased secretion of heparin sulphate proteoglycan 2 (HSPG2) which in turn improves the metastatic capacity of cancer cells [16]. Another pioneering study showed that fibroblast activating protein (FAP) expression specifically increased in CAFs upon being cultured in conditioned medium derived from colorectal cancer (CRC) cells [3].

Many techniques to track clonal dynamics have been developed over the years. Most are often limited in scope and require sufficient technical expertise to execute successfully [12]. Currently used techniques to track clonal dynamics include fluorescence activated cell sorting (FACS) or sequencing of barcoded DNA or RNA from the same source at multiple time intervals [12]. In addition, manual cell tracking via time lapse microscopy also continues to be used to track clonal populations in a spatio-temporal manner [4]. Given the inherent complexity of these techniques and the degree of subjectivity involved in the interpretation of the results obtained thereof, there is a need to develop an automated and standardized framework to reliably study clonal dynamics in a wide range of conditions [6].

Lentivirus Gene Ontology (LeGO) vectors have proven to be strong candidates that can reliably and stably transduce a wide range of primary cell cultures and established cell lines upon being packaged with the appropriate coat proteins [17]. These vectors consist of a selection of fluorescent and drug-selectable

ICCS Camera Ready Version 2023
To cite this paper please use the final published version:
DOI: 10.1007/978-3-031-36024-4_28

markers [17]. Cells can be transduced simultaneously with multiple LeGO vectors [8] to give rise to distinct cell lineages characterized by different colors [17]. The fluorescent proteins can further be co-expressed with a nucleus-localizing signal (NLS) to ensure fluorescence from a cell is restricted to its nucleus.

Given the ease with which cells can be fluorescently tagged using LeGO vectors, in this paper, we develop a novel, high-throughput image-processing framework to analyze clonal dynamics of CRC cells. We further develop a simple two function agent-based cell proliferation model to explore the effects of local density on colony growth.

2 Materials and Methods

2.1 Cell Culture HT55 (Sanger Institute) cells and primary human embryonic fibroblasts (HEFs), established previously by our lab [7], were cultured in DMEM/F12 (Life Technologies) supplemented with 1% Penicillin-Streptomycin (Gibco) and 10% fetal calf serum (FCS;Gibco). For the co-cultures, cells were cultured in DMEM/F12 (Life Technologies) supplemented with 1% Penicillin-Streptomycin (Gibco) and 0.1% fetal calf serum (Gibco). Cell lines were incubated at 37 °C and 5.0 % CO_2.

2.2 Multicolor Marking To introduce LeGO markers into the HT55 cells, we followed the techniques previously utilised by Weber et al. [18] and Heijen et al. [2]. To improve data acquisition, we inserted a nuclear localization signal of the human c-Myc proto-oncogene (3' GGACGACGCTTCTCCCAGTTTAACCTG 5') [1] into the LeGO-C2 (27339), LeGO-V2 (27340), and LeGO-Cer2 (27338) (Addgene) vectors, using standard DNA cloning protocols. This enabled nuclear visualization. Briefly, 50,000 cells were seeded in a single well of a 12-well plate in 1 mL culture medium and incubated at 37°C and 5.0% CO2 for 24 h, at 70 % confluency. The medium was refreshed with 1 mL culture medium containing 8 μg mL^{-1} polybrene (Sigma-Aldrich) and 50 μL of either LeGO or LeGO-NLS lentivirus, was added into the medium. Cells were incubated overnight at 37 °C and 5.0 % CO_2 and the medium was refreshed the next day. Transduced cells were selected by a Sony SH800 cell sorter.

2.3 Treatment assay 2000 HT55 LeGO cells were seeded in the wells of 96 wells-plate three days prior to treatment. After 3 days, cells were either treated with 2.5 µM oxaliplatin (Sigma) or 100 µM 5-fluorouracil (Sigma). Drug concentrations were based on the IC_{50} found in Genomics of Drug Sensitivity in Cancer (GDSC) database [19] and our preliminary drug response experiments. Cell lines were treated with different chemotherapy drugs for 3 days, followed by a 4 day wash out cycle and then imaged at these days.

2.4 The effect of fibroblasts on cell growth To investigate the effect of fibroblasts on cell growth, we co-cultured 1000 HT55 cells with 7000 human fibroblasts per well in a 96-well plate. As a control, 1000 HT55 cells were cultured

ICCS Camera Ready Version 2023
To cite this paper please use the final published version:
DOI: 10.1007/978-3-031-36024-4_28

without fibroblasts per well in the same 96-well plate. Three independent experiments were performed. Image acquisition was started 3 hours post-seeding and continued daily for at least 5 time points to monitor the growth of HT55 cells in the presence or absence of fibroblasts.

2.5 Imaging HT55 cells were imaged using an EVOS FL Cell Imaging System (Thermo Fisher Scientific) with a 4X objective, and the following LED light cubes were utilized: Texas Red (excitation 445/45 nm and emission 510/42 nm), YFP (excitation 500/24 nm and emission 524/27 nm), and CFP (excitation 585/29 nm and emission 624/40 nm). High resolution images were captured using a Leica Thunder Wide Field Fluorescence Microscope at 10x magnification, with the following settings: Quad Filter Block; DFT51010 or CYR70010 both of which employ an excitation wavelength of 375-412 nm, 483-501 nm, and 562-588 nm, and an emission wavelength of 441-471 nm, 512-548 nm, and 600-660 nm for mCerulean, mVenus, and mCherry respectively.

2.6 Image analysis An image processing pipeline "LeGO cell track" was developed to analyze the experimentally obtained microscopy images. First, high resolution microscopy images were exported to PNG image format. The raw PNG images were processed using ImageJ v1.53k to remove background fluorescence. An image correction method to reduce temporal background noise and shading [11] was implemented via the BaSiC plugin in ImageJ. The background corrected images were then aligned based on their temporal sequence. To enable temporal tracking, we used OpenCV's motion tracking protocol "MOTION AFFINE". The aligned images were segmented for individual bright field (black and white) segments. These segments may contain multiple colonies overlapping on each other. The identified segments were separated based on the colors of cells into individual colonies. To accomplish this color-based colony sorting, the pixel colors within a segment was clustered into eight different channels in the Hue, Saturation and Value (HSV) color map. Geometric and other statistical metrics such as the center of mass of a colony, area occupied and color channel were extracted from the color sorted colonies. These metrics were used to track individual colonies through images from different consequent time points.

2.7 Model development We developed a spatiotemporal agent-based model to quantify the clonal growth dynamics. Each agent was assumed to represent a colony. The agent attributes include cell status, grid positions, area, proximal density, distal density, and color channel. In this study, these attribute values are extracted from the experimental data for initialization. The localized attribute values of the agents enables parallel execution of the model [13] at cell level. We introduce a simple two-function model to simulate microenvironmental influence on agent proliferation.

$$\frac{da_i}{dt} = (\psi_i(\rho_p) + \phi_i(\rho_d))a_i \tag{1}$$

ICCS Camera Ready Version 2023
To cite this paper please use the final published version:
DOI: 10.1007/978-3-031-36024-4_28

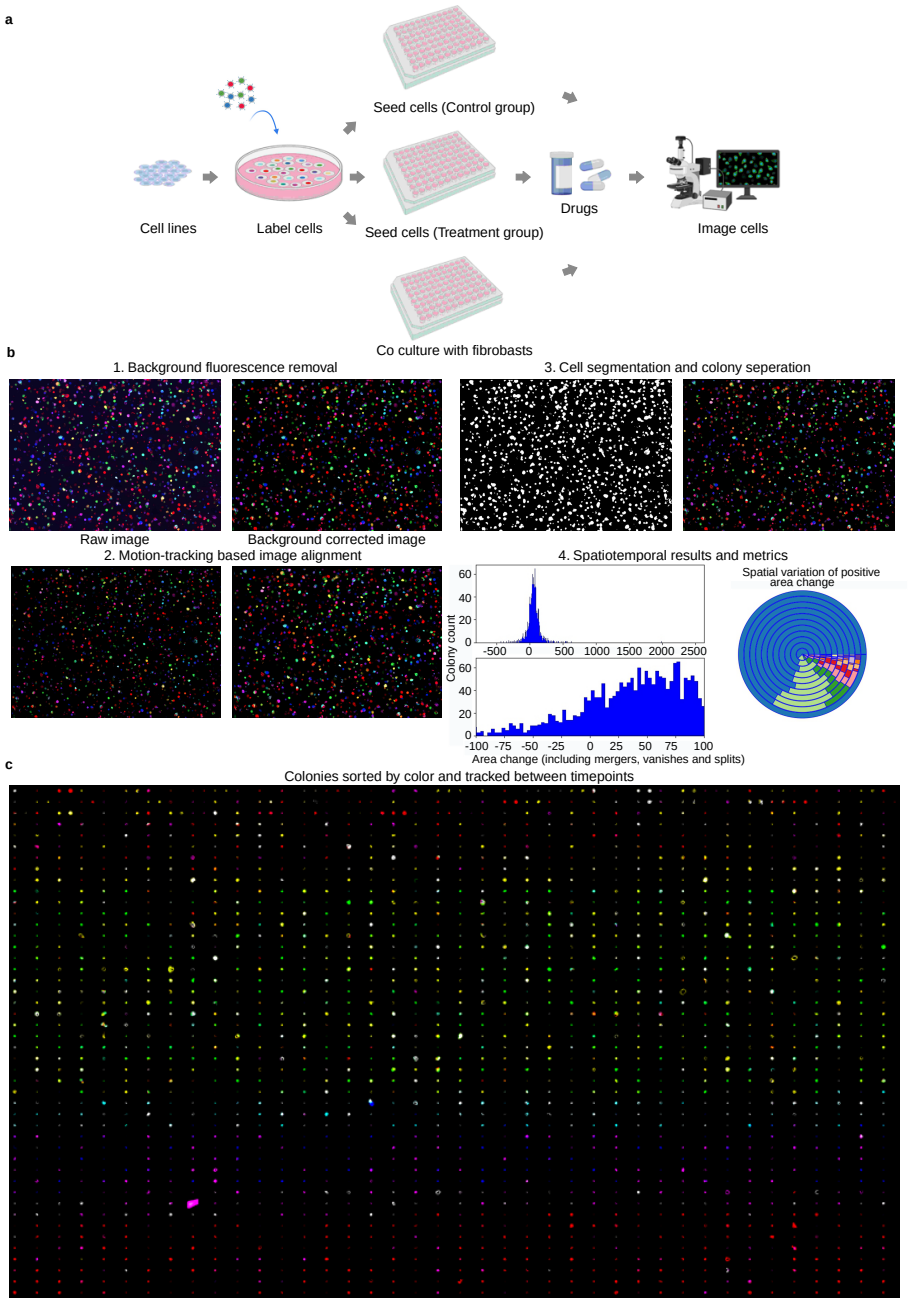

Fig. 1. Framework for automated high-throughput clonal growth tracking (a) Experimental setup illustration created with BioRender.com (b) Steps involved in processing the microscopy image data and (c) Color sorted and time-tracked colonies placed in a (time point 1, time point 2) manner.

ICCS Camera Ready Version 2023
To cite this paper please use the final published version:
DOI: 10.1007/978-3-031-36024-4_28

$$\psi_i(\rho_p) = k_1\rho_p \tag{2}$$

$$\phi_i(\rho_d) = k_2\rho_d \tag{3}$$

The clonal area of a cell a_i is quantified based on equation 1 where, ψ_i and ϕ_i are proximal and distal density-based growth contributions respectively from the microenvironment, ρ_p and ρ_d indicate the proximal and distal densities respectively. The densities are calculated as ratio of area occupied by clones within a zone to the total area of the zone. k_1 and k_2 from equations 2 and 3 are rate constants denoting contribution to area-growth per unit density at proximal and distal levels.

$$S_i = \begin{cases} 1, & \text{if } a_i > m \\ 0, & \text{otherwise} \end{cases} \tag{4}$$

The status of an agent is classified as viable (1) or extinct (0) based equation 4. Here, m is an area constant below which a cell is considered dead. In this study, m = 14 grids, which is the minimum area cutoff for a clone in experiments.

For model parametric fitting, we extracted a smaller (nx*ny) 1000x1000 area from EXP67 microscopy images to limit compute resource requirements for the fitting process. The radius for proximal and distal density measurements were fixed at approximately 1/3 of image length and full image length respectively.

A loss function indicated in equation 5 was minimized to carry out the parametric fitting,

$$\chi = M_{SE}(\sum a_i, \overline{\rho_p}, \overline{\rho_d}, med(\rho_p), med(\rho_d)) \tag{5}$$

In equation 5, χ indicates the loss, M_{SE} indicates the mean square error, $\sum a_i$ represents the sum of colony areas, $\overline{\rho_p}$,$\overline{\rho_d}$ are the mean proximal and distal densities respectively and $med(\rho_p)$,$med(\rho_d)$ are the median proximal and distal densities respectively.

3 Results and discussions

In order to analyze the clonal dynamics of HT55 cells cultured as mono-cultures (with the addition or omission of 5-FU or Oxaliplatin) or co-cultures (in the presence or absence of fibroblasts), LeGO labeled HT55 cells were seeded in well plates corresponding to different experimental conditions (Figure 1a). Cells cultured as mono-cultures were imaged at varying time points with or without cytotoxic drugs. For the co-cultures, seeded cells within the same plate were cultured with or without fibroblasts and imaged at multiple time points up to eight days post-seeding. Figure 1b highlights the framework through which clones across different conditions were tracked over time. The background of the raw images obtained at different time intervals were first corrected to remove excess fluorescence arising from additional constituents of the microenvironment such as fibroblasts or added cytotoxic agents. The background corrected images from two time points were then aligned on the basis of colony motion-tracking (see section 2.6). Irrespective of the distinct and varied fluorescent colors expressed by

ICCS Camera Ready Version 2023
To cite this paper please use the final published version:
DOI: 10.1007/978-3-031-36024-4_28

colonies, the motion-tracking technique employed was able to reliably segregate individual colonies (Figure 1c). Following colony motion-tracking, clones were separated and color sorted on the basis of their fluorescence (Figure 1b). The developed high-throughput framework was first benchmarked against synthetic microscopy images with known cell count and area increase. A seed image with dimensions similar to the experimental images (5439 x 3238 pixels) was constructed with a random distribution of 100 colonies of equal area of disc shape. To mimic colony growth, two additional synthetic images were created. These images use the same seed positions of colonies from the seed image but with equal incremental area coverage of the individual colonies as shown in figure 2a (t1, t2 and t3). The colony sizes were varied in a linear fashion (1x, 2x and 3x) with respect to the disc radius in the synthetic images generated at the three time points (t1, t2 and t3). There was no overlap of colonies in the first two synthetic images (interval 1). In the second and third synthetic images (interval 2) two colonies overlapped over each other. Analytically estimated ratio of area increase between the intervals was 1.67. These three synthetic images were analyzed with the presented framework. As expected, there is no variation in colony number with time and total colony count remains at 100 as evidenced in figure 2b and figure 2d. Figure 2c provides a comparison of area increase between different intervals. The framework overestimated the ratio of area increase by approximately 11% compared to the analytical solution. This could potentially be due to image compression artifacts when creating the synthetic images. Overall, the benchmarking of the developed framework against synthetic images shows that it segments and tracks with sufficient accuracy in an ideal setting. Additionally, the framework is capable of handling overlap of colonies by separating and color sorting them into individual colonies.

Throughout the study we used three major clonal growth indicators, (i) area increase per area - calculated as ratio of area increase between time points (interval) to the area occupied by the colonies at the start of the interval, (ii) area increase per colony - calculated as ratio of area increase between time points (interval) to the number of colonies at the start of the interval and (iii) area increase - indicating total area change between a period of time. Negative values indicate decrease in colony area. In the control conditions of the mono-culture drug experiments, a consistent reduction in area increase per area was observed upon increase of total area and normalized neighbor area of clonal colonies (Figures 2e, 3g, 3i, 3k, 3m, 3o, 3q) despite experiment 5 behaving as an outlier. The same phenomenon was observed when comparing area increase per area to the total number of clonal colonies (Figures 2f, 3h, 3j, 3l, 3n, 3p, 3r). These results show that overall area increase would be lesser in densely packed or confluent systems. However, if we consider local density effects on the clonal growth, the trend reverses. In figures 3g-3r, we observe that there is a consistent increase in clonal growth in colonies with maximum clonal density surrounding them at intra-day level. In addition, in most experiments, we see a gradual increase of growth indicators in the heat maps especially at earlier time points (Figures 3g-3r) suggesting a directly proportional relationship between local clonal density

ICCS Camera Ready Version 2023
To cite this paper please use the final published version:
DOI: 10.1007/978-3-031-36024-4_28

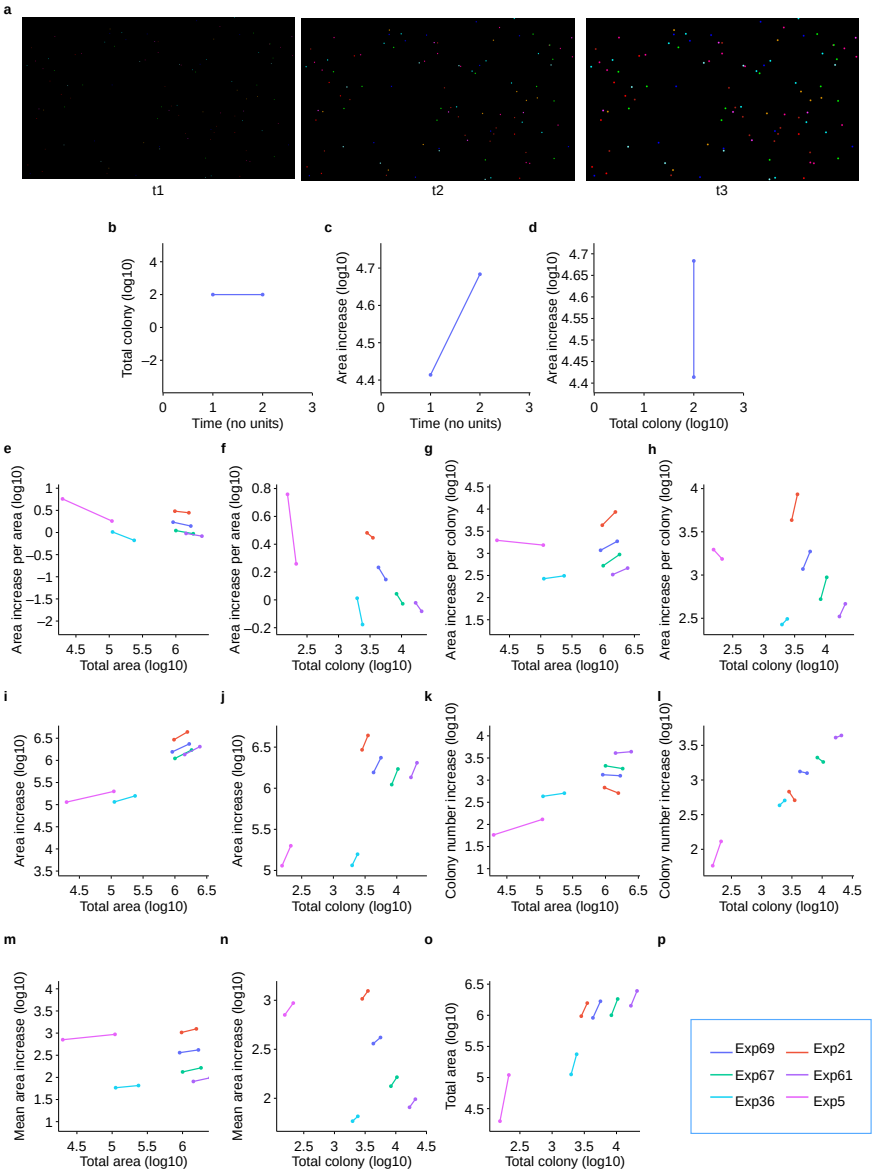

Fig. 2. Clonal proliferation profiles resulting from mono-culture experiments,(a) Synthetic images for different timepoints (b), (c), (d) are comparisons of various growth parameters for synthetic images, (e) – (o) plots of growth indicators for the control conditions of the mono-culture drug experiments and (p) figure legend for plots (e) – (o).

ICCS Camera Ready Version 2023
To cite this paper please use the final published version:
DOI: 10.1007/978-3-031-36024-4_28

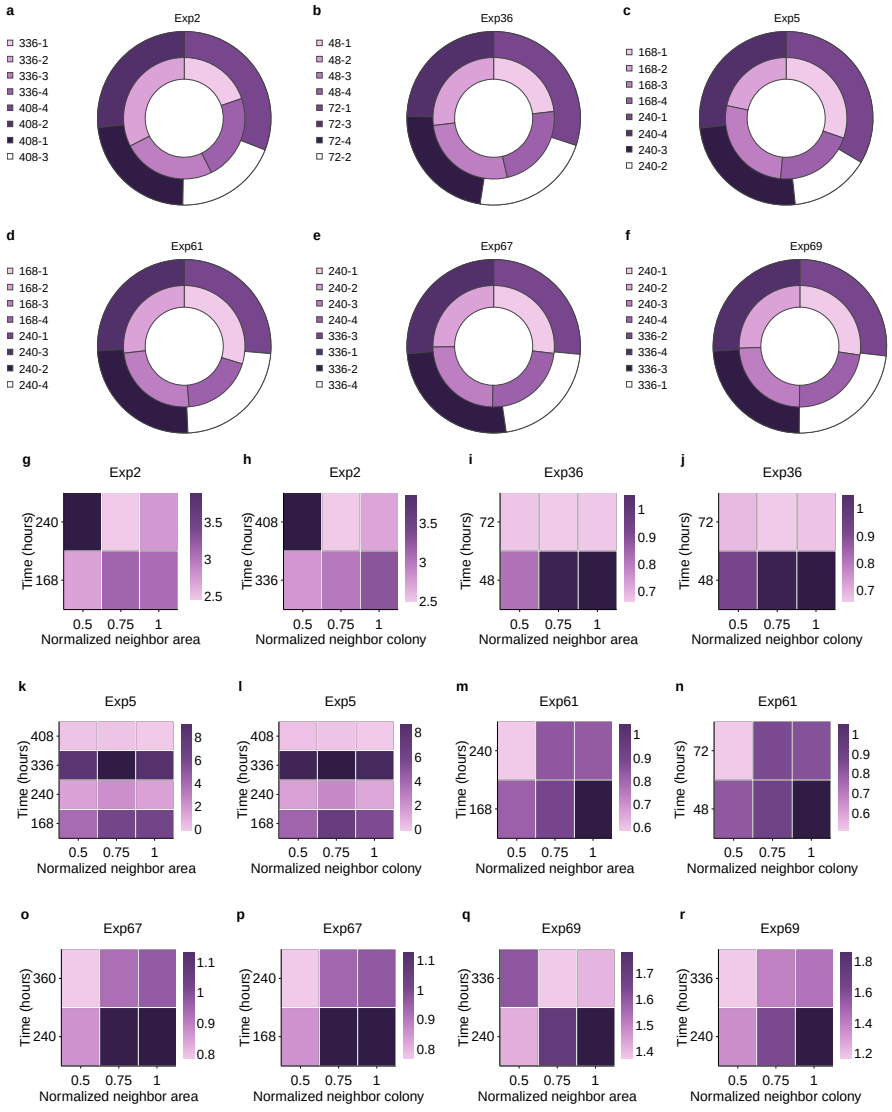

Fig. 3. Temporal and spatial variations of clonal proliferation resulting from monoculture experiments, (a) – (f) Concentric area profiles for area increase per area for different time points and control experiments, the gradients indicate the magnitude of area change per area and the legends indicate the 'time point - the relative concentric area position' in the experiments and (g) – (r) heatmaps showing the variations in area increase per area at various normalized density zones (neighbor area and neighbor colony count) for different time points and control experiments.

ICCS Camera Ready Version 2023
To cite this paper please use the final published version:
DOI: 10.1007/978-3-031-36024-4_28

and clonal growth. Area increase per clonal colony in relation to an increase in either total area or total number of clonal colonies was observed to also increase in an unexpectedly linear manner (Figures 2g, 2h). This is indicative of few mitotic cells being able to branch off from a clonal colony to form new colonies. Instead, these cells stay within their colony of origin and divide to lead to an increase in clonal colony area. An overall trend of increasing area compared to increase in either total area or total number of cells is further observed (Figures 2i, 2j). Correlation between clonal colony number increase and total area or total number of clonal colonies was not well established (Figures 2k and 2l). These results support previous results (Figures 2b, 2d, 2g, 2h) and show that the spontaneous formation of new clonal colonies over time is unlikely despite growth of the established colonies. While the area increase per area in relation to total area or number of clonal colonies showed a negative trend, the other parameters showed an increasing trend on average. This is reflected by the mean area increase plots (Figure 2m, 2n). Figure 2o shows a positive correlation between total area and total clonal colonies over time, as is expected.

To estimate the influence of growth solutes on clonal proliferation and ascertain the presence of any diffusion limitations, we calculated the clonal growth parameters within different concentric area profiles shown in figures 3a - 3f. The total area in the image was split into four zones (1,2,3 and 4), which are enclosed within concentric circles of four different radii. The maximum radius of the circle was fixed to the width of the microscopy image. The reminder radii were calculated as normalized values of 0.25, 0.5 and 0.75 of the maximum radius. Area increase per area in these zones were then calculated to analyze if there were variations in growth between the zones. The results from the analysis are summarized in figures 3a-3f for different experiments. The zones from the concentric area are represented as sectors in the circle, with the innermost zone to the outer zone arranged as they would be within wells.

If there were diffusion limitations in the system, then one or more of these sectors should occupy most area of the circle due to presence of local clonal hotspots. However, no such asymmetry is observed in the circles and the zones are found to exhibit similar area increase per area. This eliminates the presence of diffusion limitation zones and the cells in the experiment may be assumed to grow in the presence of excess nutrients. We analyzed the effects of two drugs 5-FU and Oxaliplatin on the proliferation of clonal colonies. Negative clonal growth indicators were observed in the drug treated clonal growth analysis. Figures 4e-4h and 4m-4n summarize the changes in clonal growth. Other than the one outlier in figure 4h (area increase) all other plots show consistent decrease in clonal growth both in terms of clonal area and colony count. Density dependent growth contribution was not observed from the heatmaps 4a - 4d and 4i-4l. Overall, drug treated systems behave vastly dissimilar to the control population in terms of clonal growth and local and global density-driven effects. Clonal colony dynamics were also studied in co-cultures to ascertain the effect of fibroblasts on HT55 colonies in vitro (Figure 5). Area increase was observed to be reduced in the mono-culture condition while the opposite trend was observed in

ICCS Camera Ready Version 2023
To cite this paper please use the final published version:
DOI: 10.1007/978-3-031-36024-4_28

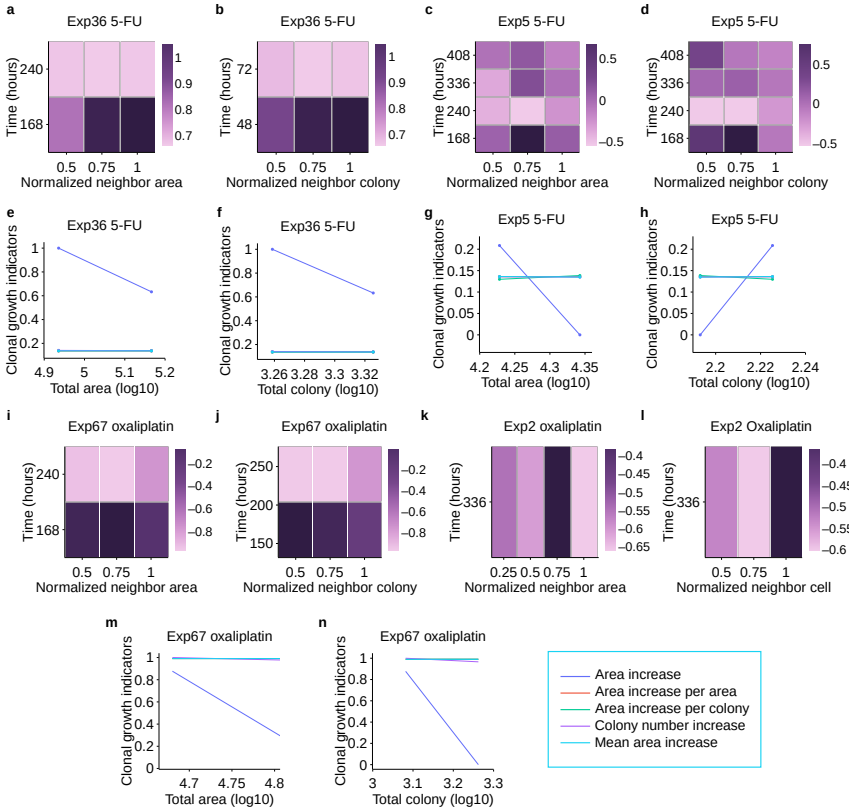

Fig. 4. Effect of spatial density on drug treated clonal growth (a)-(d) Heatmaps showing the variations in area increase per area at various normalized density zones for different time points and 5-FU experiments, (e) – (h) clonal growth indicators at different time points for 5-FU experiments, (i)-(l) heatmaps showing the variations in area increase per area at various normalized density zones for different time points and oxaliplatin experiments, (m) – (n) clonal growth indicators at different time points for oxaliplatin experiment. The clonal growth indicators are included in the figure legend.

ICCS Camera Ready Version 2023
To cite this paper please use the final published version:
DOI: 10.1007/978-3-031-36024-4_28

the case of the co-culture condition (Figure 5a). Similar to the control results of the cytotoxic drug experiment presented in figure 2, a reduction in area increase per area was observed over time in the mono- and co-culture condition, albeit to a lesser extent in the case of the co-culture condition (Figure 5b). Area increase per clonal colony was also observed in both conditions (Figure 5c), in line with expectations based on figure 2. While the clonal colony number increase remained similar over time for the mono-culture condition, a marked decrease was observed in the co-culture condition (Figure 5d). This observation might be due to the mono-culture condition being less confluent therefore, supporting the spontaneous formation of new clonal colonies for a longer interval of time. Furthermore, the mean area increase over time was reduced in both conditions (Figure 5e) and was lower in the co-culture condition suggesting confluency is attained faster in the presence of fibroblasts . Taken together, these results suggest that similar to the control HT55 cultures in the cytotoxic drug experiments, confluent co-culture systems also exhibit overall reduced area increase over time. Additionally, the results support the notion that fibroblasts produce factors to create a pro-clonal colony environment which supports faster clonal outgrowth. The agent-based model was numerically simulated using the experimental findings as input for model initialization. Three time points 168, 240 and 360 h from Exp67 were used for parametric quantification. Loss functions were minimized for two different time intervals I (168-240) and II (240-336). To include intermediate density-driven dynamics between the large intervals, one hour was chosen as the minimum time step Δt for the simulations. Loss minimization landscape is summarized in figure 5f and 5g . The z-axis of the plots is set in log scale to capture the vast range of loss values. In both intervals I and II multiple local minima can be observed. The values of k1 and k2 are positive and negative respectively indicating the contributions to total area change from the proximal and distal clonal densities. The values of k1 and k2 at different time intervals I and II are k1 (I) = 0.08, k1 (II) 0.021, k2 (I) = -0.061 and k2(II) =-0.013. Values of k1 decreases with time while k2 increases. Thus, in the simple two-function clonal growth model, k1 may be considered as the growth contribution factor, while k2 as a growth retardation parameter. The numerical range of model parameters, k1 and k2, do not exhibit drastic change between the different intervals of growth analyzed. This is an expected behavior since the density effects cannot drive overall clonal proliferation higher than its threshold growth capacity and nutrient availability. The contribution to growth retardation by parameter k2 increases with time indicating the increase in energy requirement for overall clonal growth. Therefore, k1 and k2, may be treated as energy requirement parameters varying based on the cell type. Both k1 and k2, are seen to tend towards the value of 0 with approximately equal rate of change. This is reflected in the heatmaps of figures 3g, k and o, where, at later time points, clonal density does not play a significant role in clonal growth as growth saturates. The developed nutrient-independent model could enable simulation of tumor proliferation through elimination of computationally intensive mass-transfer kinetics modelling [5][14]. Even though the simple two-function model can capture the

ICCS Camera Ready Version 2023
To cite this paper please use the final published version:
DOI: 10.1007/978-3-031-36024-4_28

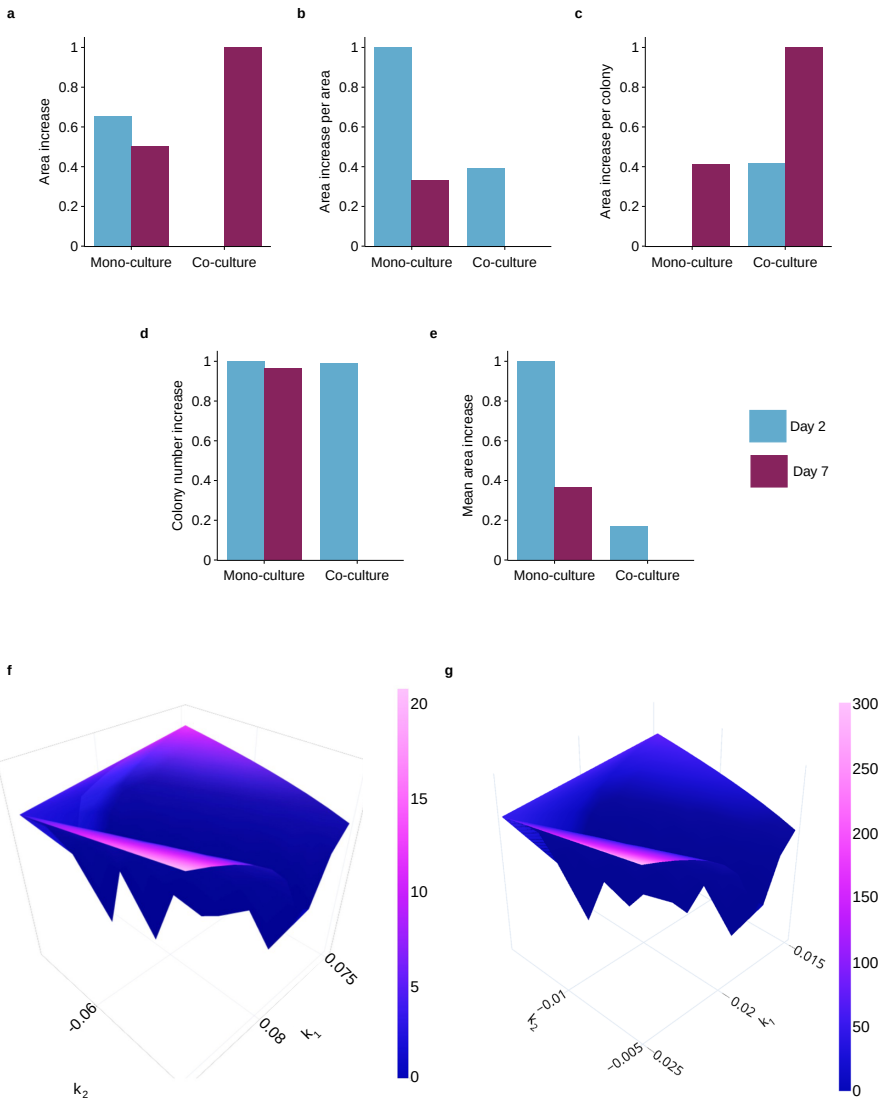

Fig. 5. Comparison of clonal growth indicators between mono- and co-culture systems (a)-(e) at different time points, the clonal growth indicators are normalized between 0-1 at different time points and (f) and (g) loss function minimization landscape for k1 and k2 parameters in the computational model, the color bar indicates the loss calculated from the χ function.

ICCS Camera Ready Version 2023
To cite this paper please use the final published version:
DOI: 10.1007/978-3-031-36024-4_28

growth contributions from proximal and distal densities, the current model is restricted to systems with presence of excess nutrients. In presence of a limiting solute, clonal growth would be restricted by diffusion dynamics. One other limitation of the current agent-based model is that area overlap between clones is not considered. This could mean that loss function minimization may not result in a global minimum and produce underestimated parametric values.

4 Conclusions

We developed a high throughput framework for clonal tracking and growth estimation. From the framework outputs, we discovered that local density of clones could affect the growth rate of the colonies. To test this hypothesis, a simple two function agent-based model of clonal proliferation was developed. The model parameters were estimated through loss minimization principles, using inputs from the clonal growth experiments. Parameters k1 and k2 provide a straight-forward way of simulating clonal growth based on proximal and distal clonal area densities. Both k1 and k2 tend towards zero with progress of time, in the model parametric estimations, indicating a possible diminishing effect of local density in confluent older colonies. The developed model currently lacks mechanistic descriptions to simulate drug interactions and capture presence of supporting factors such as fibroblasts. As part of the future work, the model can be improved with provisions for including cell growth promoting or retarding factor(s) that are derived or inferred from the framework outputs.

References

1. Dang, C.V., Lee, W.: Identification of the human c-myc protein nuclear translocation signal. Molecular and cellular biology **8**(10), 4048–4054 (1988)
2. van der Heijden, M., Miedema, D.M., Waclaw, B., Veenstra, V.L., Lecca, M.C., Nijman, L.E., van Dijk, E., van Neerven, S.M., Lodestijn, S.C., Lenos, K.J.: Spatiotemporal regulation of clonogenicity in colorectal cancer xenografts. Proceedings of the National Academy of Sciences **116**(13), 6140–6145 (2019)
3. Henriksson, M.L., Edin, S., Dahlin, A.M., Oldenborg, P.A., Öberg, A., Van Guelpen, B., Rutegård, J., Stenling, R., Palmqvist, R.: Colorectal cancer cells activate adjacent fibroblasts resulting in fgf1/fgfr3 signaling and increased invasion. The American journal of pathology **178**(3), 1387–1394 (2011)
4. Huth, J., Buchholz, M., Kraus, J.M., Schmucker, M., Von Wichert, G., Krndija, D., Seufferlein, T., Gress, T.M., Kestler, H.A.: Significantly improved precision of cell migration analysis in time-lapse video microscopy through use of a fully automated tracking system. BMC cell biology **11**, 1–12 (2010)
5. Kaura, P., Mishra, T., Verma, N., Dalal, I.S., Sheraton, V.: Effects of combined chemotherapeutic drugs on the growth and survival of cancerous tumours–an in-silico study. Journal of Computational Science **54**, 101421 (2021)
6. Kok, R.N., Hebert, L., Huelsz-Prince, G., Goos, Y.J., Zheng, X., Bozek, K., Stephens, G.J., Tans, S.J., Van Zon, J.S.: Organoidtracker: Efficient cell tracking using machine learning and manual error correction. PLoS One **15**(10), e0240802 (2020)

ICCS Camera Ready Version 2023
To cite this paper please use the final published version:
DOI: 10.1007/978-3-031-36024-4_28

7. Lenos, K.J., Miedema, D.M., Lodestijn, S.C., Nijman, L.E., van den Bosch, T., Romero Ros, X., Lourenco, F.C., Lecca, M.C., van der Heijden, M., van Neerven, S.M.: Stem cell functionality is microenvironmentally defined during tumour expansion and therapy response in colon cancer. Nature cell biology **20**(10), 1193–1202 (2018)
8. Mohme, M., Maire, C.L., Riecken, K., Zapf, S., Aranyossy, T., Westphal, M., Lamszus, K., Fehse, B.: Optical barcoding for single-clone tracking to study tumor heterogeneity. Molecular Therapy **25**(3), 621–633 (2017)
9. Mulkearns-Hubert, E.E., Torre-Healy, L.A., Silver, D.J., Eurich, J.T., Bayik, D., Serbinowski, E., Hitomi, M., Zhou, J., Przychodzen, B., Zhang, R.: Development of a cx46 targeting strategy for cancer stem cells. Cell reports **27**(4), 1062–1072. e5 (2019)
10. Noonan, J., Grassia, G., MacRitchie, N., Garside, P., Guzik, T.J., Bradshaw, A.C., Maffia, P.: A novel triple-cell two-dimensional model to study immune-vascular interplay in atherosclerosis. Frontiers in Immunology **10**, 849 (2019)
11. Peng, T., Thorn, K., Schroeder, T., Wang, L., Theis, F.J., Marr, C., Navab, N.: A basic tool for background and shading correction of optical microscopy images. Nature communications **8**(1), 14836 (2017)
12. Pogorelyy, M.V., Minervina, A.A., Touzel, M.P., Sycheva, A.L., Komech, E.A., Kovalenko, E.I., Karganova, G.G., Egorov, E.S., Komkov, A.Y., Chudakov, D.M.: Precise tracking of vaccine-responding t cell clones reveals convergent and personalized response in identical twins. Proceedings of the National Academy of Sciences **115**(50), 12704–12709 (2018)
13. Sheraton, M.V., Sloot, P.M.: Parallel performance analysis of bacterial biofilm simulation models. In: Computational Science–ICCS 2018: 18th International Conference, Wuxi, China, June 11–13, 2018, Proceedings, Part I 18. pp. 496–505. Springer (2018)
14. Sheraton, V.M., Ma, S.: Exploring ductal carcinoma in-situ to invasive ductal carcinoma transitions using energy minimization principles. In: Computational Science–ICCS 2022: 22nd International Conference, London, UK, June 21–23, 2022, Proceedings, Part I. pp. 375–388. Springer (2022)
15. Tang, R., Murray, C.W., Linde, I.L., Kramer, N.J., Lyu, Z., Tsai, M.K., Chen, L.C., Cai, H., Gitler, A.D., Engleman, E.: A versatile system to record cell-cell interactions. Elife **9**, e61080 (2020)
16. Vennin, C., Mélénec, P., Rouet, R., Nobis, M., Cazet, A.S., Murphy, K.J., Herrmann, D., Reed, D.A., Lucas, M.C., Warren, S.C.: Caf hierarchy driven by pancreatic cancer cell p53-status creates a pro-metastatic and chemoresistant environment via perlecan. Nature communications **10**(1), 3637 (2019)
17. Weber, K., Bartsch, U., Stocking, C., Fehse, B.: A multicolor panel of novel lentiviral "gene ontology"(lego) vectors for functional gene analysis. Molecular therapy **16**(4), 698–706 (2008)
18. Weber, K., Thomaschewski, M., Benten, D., Fehse, B.: Rgb marking with lentiviral vectors for multicolor clonal cell tracking. Nature protocols **7**(5), 839–849 (2012)
19. Yang, W., Soares, J., Greninger, P., Edelman, E.J., Lightfoot, H., Forbes, S., Bindal, N., Beare, D., Smith, J.A., Thompson, I.R.: Genomics of drug sensitivity in cancer (gdsc): a resource for therapeutic biomarker discovery in cancer cells. Nucleic acids research **41**(D1), D955–D961 (2012)
20. Zhu, J., Thompson, C.B.: Metabolic regulation of cell growth and proliferation. Nature reviews Molecular cell biology **20**(7), 436–450 (2019)

ICCS Camera Ready Version 2023
To cite this paper please use the final published version:
DOI: 10.1007/978-3-031-36024-4_28